Title

Selective block of human Kv1.1 channels and an epilepsy-associated gain-of-function mutation by AETX-K peptide.

Journal

Federation proceedings, 38(1)

Authors

Zhao, Ruiming
Qasim, Arwa
Sophanpanichkul, Punyanuch
et al.

Publication Date

2024

DOI

10.1096/fj.202302061R

Peer reviewed

Published in final edited form as:

FASEB J. 2024 January ; 38(1): e23381. doi:10.1096/fj.202302061R.

Selective block of human Kv1.1 channels and an epilepsy-associated gain-of-function mutation by AETX-K peptide

Ruiming Zhao[1,*], **Arwa Qasim**[2,*], **Punyanuch Sophanpanichkul**[1], **Hui Dai**[1], **Maha Nayak**[1], **Inbal Sher**[2], **Jordan Chill**[2], **Steve A. N. Goldstein**[1]

[1]Departments of Pediatrics, Physiology & Biophysics, and Pharmaceutical Sciences, Susan and Henry Samueli College of Health Sciences, University of California, Irvine, Irvine, CA 92697, USA

[2]Department of Chemistry, Bar Ilan University, Ramat Gan, 52900, Israel

Abstract

Dysfunction of the human voltage-gated K^+ channel Kv1.1 has been associated with epilepsy, multiple sclerosis, episodic ataxia, myokymia, and cardiorespiratory dysregulation. We report here that AETX-K, a sea anemone type I (SAK1) peptide toxin we isolated from a phage display library, blocks Kv1.1 with high affinity (K_i ~1.6 pM) and notable specificity, inhibiting other Kv channels we tested a million-fold less well. Nuclear magnetic resonance (NMR) was employed both to determine the three-dimensional structure of AETX-K, showing it to employ a classic SAK1 scaffold while exhibiting a unique electrostatic potential surface, and to visualize AETX-K bound to the Kv1.1 pore domain embedded in lipoprotein nanodiscs. Study of Kv1.1 in *Xenopus* oocytes with AETX-K and point variants using electrophysiology demonstrated the blocking mechanism to employ a toxin-channel configuration we have described before whereby AETX-K Lys_{23}, two positions away on the toxin interaction surface from the classical blocking residue, enters the pore deeply enough to interact with K^+ ions traversing the pathway from the opposite side of the membrane. The mutant channel Kv1.1-L_{296}F is associated with pharmaco-resistant multifocal epilepsy in infants because it significantly increases K^+ currents by facilitating opening and slowing closure of the channels. Consistent with the therapeutic potential of AETX-K for Kv1.1 gain-of-function-associated diseases, AETX-K at 4 pM decreased Kv1.1-L_{296}F currents to wild-type levels; further, populations of heteromeric channels formed by co-expression Kv1.1 and Kv1.2, as found in many neurons, showed a K_i of ~10 nM even though homomeric Kv1.2 channels were insensitive to the toxin (K_i >2000 nM).

Graphical Abstract

Correspondence: Ruiming Zhao, ruimiz3@uci.edu; Jordan Chill, jordan.chill@biu.ac.il.

*These authors contributed equally to this article.

AUTHOR CONTRIBUTIONS

Ruiming Zhao, Jordan Chill and Steve A. N. Goldstein designed research; Ruiming Zhao, Arwa Qasim, Punyanuch Sophanpanichkul, Hui Dai, Maha Nayak, Inbal Sher performed research; Ruiming Zhao, Jordan Chill and Steve A. N. Goldstein wrote the article.

DISCLOSURES

The authors declare that they have no conflicts of interest with the contents of this article.

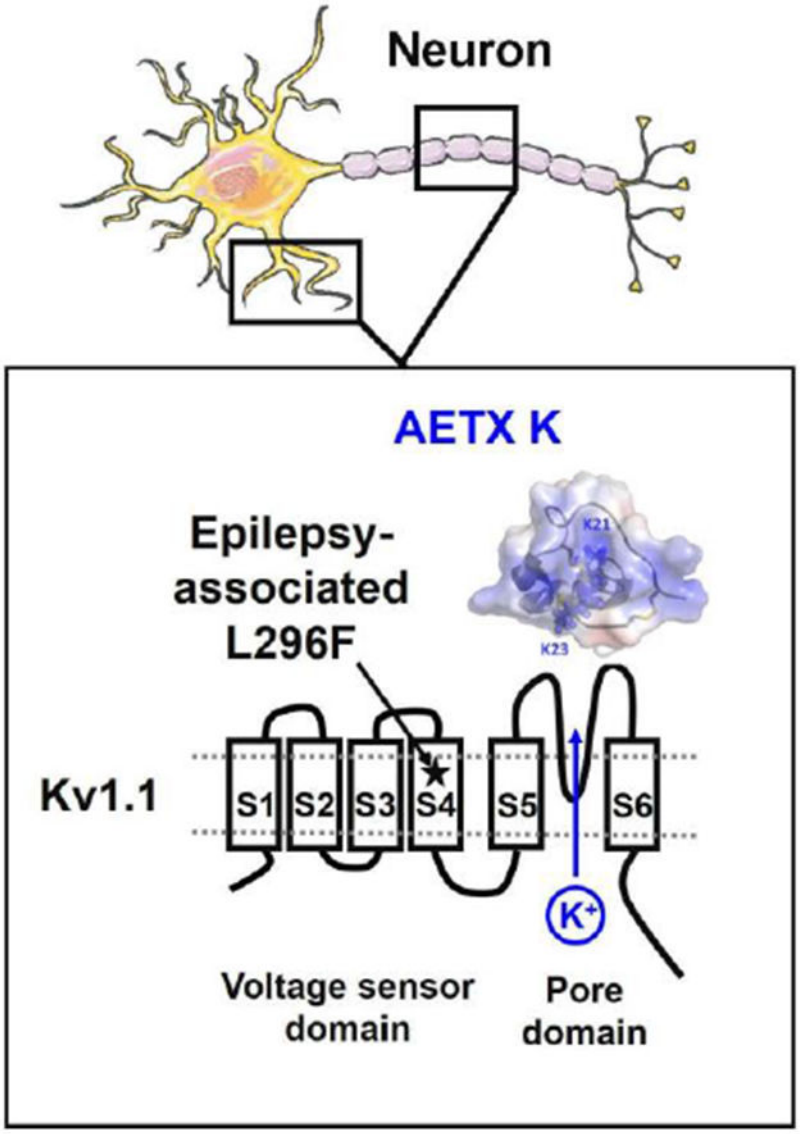

Keywords

AETX-K; venom peptide; Kv1.1; NMR; epilepsy

1 | INTRODUCTION

The voltage-gated K^+ channel Kv1.1 is expressed across the human central nervous system, prominently in the hippocampus, cerebellum, and neocortex (1, 2). In neurons, Kv1.1 channels regulate the threshold of action potential generation, action potential repolarization, firing frequency, and thereby neurotransmitter release (3). Kv1.1 channels are composed of four subunits and can assemble as homotetramers or mixed complexes, notably with Kv1.2 (3). Each Kv1.1 subunit contains six transmembrane segments (S1-S6), S1-S4 comprise the voltage sensor domain (VSD), and S5-S6 forms the pore domain that allows transmembrane

flux of K^+ ions when the channel opens on membrane depolarization (Figure 1B) (3). A spectrum of neurological diseases has been associated with mutations in the KCNA1 gene encoding for Kv1.1 channels. These include more than 40 loss-of-function mutations linked to episodic ataxia type 1, paroxysmal kinesigenic dyskinesia, hypomagnesemia, and epilepsy (1). Increased Kv1.1 channel activity has been associated with multiple sclerosis (4) and, recently, severe, pharmaco-resistant multifocal epilepsy in an infant with a gain-of-function mutation, Kv1.1-$L_{296}F$ (5). The patient was not sensitive to maximal therapeutic doses of anti-seizure medications, whereas compassionate use of 4-aminopyridine (4-AP) reduced seizure burden and prevented rehospitalization. Unfortunately, 4-AP blocks Kv1.1 only at μM levels, cross-reacts with other channels in the Kv1 subfamily (6), and can be toxic, causing diaphoresis, altered mental status, and seizures with dopamine-related movement abnormalities including tremor, choreoathetosis, and dystonia (7). A blocker with greater specificity and higher affinity for Kv1.1 might be beneficial for patients with gain-of-function-associated diseases like this child (5, 8).

Sea anemones are a rich source of peptide toxins that block K^+ channels; the peptides have been used as tools to study the structure and function of K^+ channels and are being explored as therapeutic agents for diseases including multiple sclerosis, psoriasis, and rheumatoid arthritis (9). Previously, we identified three blockers of the bacterial KcsA K^+ channel, HmK, Hui1 and AETX-K (Figure 1A), by screening a phage display library of 1.5 million combinatorial variants of sea anemone type I (SAK1) peptides created based on the sequences of 150 SAK1 toxin genes (10). KcsA exhibits high sequence and structural homology to the S5-S6 domain of voltage gated K^+ (Kv) channels (11). We observed that HmK, a natural toxin in the library isolated from the sea anemone *Heterotactica magnifica*, was potent but promiscuous, blocking KcsA, human Kv1.2, human Kv1.3, and Shaker channels with half-maximal equilibrium inhibition constants (K_i) of 1 to 4 nM (10, 12). HmK blocks from the external side of the membrane by occluding the conduction pore with Lys_{22}, a lysine conserved across the SAK1 family, thereby conferring voltage dependence to dissociation of the toxin from its binding site because K^+ ions traversing the pore from the cytosol “knock-off” the toxin (Figure 1A and B) (12). The blocking mechanism of HmK is reminiscent of the α-KTx scorpion toxins, like charybdotoxin (CTX) and Kaliotoxin (KTx), that block Kv channels by position a conserved Lys in the outer pore vestibule to impede the passage of ions (13–15). The classical α-KTx mechanism was visualized in the crystal structure of CTX and Kv1.2, showing the ε-amino group of CTX-Lys_{27} near the first K^+ binding site in the conduction pore (16). In contrast, the novel chimeric peptide Hui1, comprised of segments from AETX-K and HmK (Figure 1A), blocked KcsA with high affinity and specificity in an unexpected manner such that Hui-Arg_{23} conferred voltage sensitivity to peptide dissociation from the outer pore vestibule, a larger basic residue located two positions away from the classical site (Figure 1B) (10).

Here, we study the natural SAKI toxin AETX-K with six Kv channels observing that it blocks Kv1.1 with high affinity (K_i ~ 1.6 pM) and notable specificity. Nuclear magnetic resonance (NMR) showed that AETX-K has the helix-kink-helix conformation, constrained by Cys11-Cys27 and Cys16-Cys31 disulfide bonds, observed for other SAK1 toxins. However, the electrostatic potential of the AETX-K binding surface presented to the channel vestibule is like that of Hui1 (that exhibits 88% sequence identity with AETX-K) but differs

considerably from HmK. Further, we find that AETX-K-Lys$_{23}$, a residue that corresponds to Hui1-Arg$_{23}$, is responsible for the voltage dependence of peptide dissociation rather than AETX-K-Lys$_{21}$ that corresponds to HmK-Lys$_{22}$, supporting the notion that AETX-K blocks in an alternative orientation like Hui1 rather than HmK.

The gain-of-function mutation Kv1.1-L296F shifts channel activation to more negative voltages, increasing current amplitude and slowing channel closure compared to wild type (WT) Kv1.1. AETX-K blocks Kv1.1-L$_{296}$F with a K_i of ~ 2.1 pM and application of 4 pM AETX-K inhibits the current of the mutant channel to WT levels. Kv1.1 can form mixed channels with other Kv1 subunits, predominantly Kv1.2, in neuronal membranes (3). AETX-K blocks populations of Kv1.1-Kv1.2 heteromeric channels formed by equal cRNA concentrations of the two subunits in oocytes with a K_i of ~ 10 nM even though Kv1.2 channels are insensitive to the toxin. The extent of the block of Kv1.1-Kv1.2 channels by various concentrations of AETX-K allows an estimation of the K_i for heteromeric channels formed with three, two and one Kv1.1 subunits of ~ 56 pM, 14 nM, and 1155 nM, respectively. We suggest that AETX-K will find utility as a tool to study the physiology and biophysics of Kv1.1 channels and can serve as a lead for medications to treat diseases associated with excess activity of channels formed with Kv1.1.

2 | MATERIALS AND METHODS

2.1 | Molecular biology

Human Kv1.1 (NM_000217), Kv1.2 (NM_004974), Kv1.3 (NM_002232), Kv1.5 (NM_002234), Kv7.2 (NM_001382235) and Kv7.3 (NM_001204824) were cloned in pMAX+ vector with the 5' and 3' portions of the *Xenopus laevis* β-globin gene, and a T7-promoter for *in vitro* transcription. Point mutation for the Kv1.1 channel was introduced using QuikChange Site-Directed Mutagenesis Kit (Agilent). The sequences of all constructs were confirmed by DNA sequencing. cRNAs for all K^+ channels were synthesized *in vitro*. The plasmids were linearized using Pme1 (New England BioLabs), purified using QIAquick PCR Purification Kit (QIAGEN), and cRNAs synthesized using the mMESSAGE mMACHINE kit for T7 (Invitrogen). cRNAs were diluted with RNase-free water, and concentrations were measured using NanoDrop 2000 (ThermoFisher Scientific) and stored at −80°C until use.

2.2 | Peptide toxin synthesis and recombinant expression

AETX-K (Q0EAE5), AETX-K-K$_{21}$N, AETX-K-K$_{23}$N, HmK (O16846) were purchased as synthetic peptides from CSBio where peptide folding reactions were quenched by acidification, products purified by reverse-phase HPLC and evaluated by mass spectral analysis, as before (10, 12). Peptides had greater than 90% purity were lyophilized and stored at −20 °C. Peptides were dissolved in recording solution for TEVC before use. ^{15}N-labeled AETX-K for assignment of chemical shifts and structure determination was expressed by modifying previously reported protocols (17). Briefly, a Trx-TEV-AETX-K fusion construct was expressed in *E. coli* BL21(DE3) inclusion bodies (IB) using M9 minimal medium supplemented with 100 mg/mL ampicillin and containing 1 g/L $^{15}NH_4Cl$ and 4 g/L glucose. After cell lysis and pelleting of the IB, they were solubilized in buffer

containing 6M guanidine-HCl and 2 mM dithiothreitol (DTT) and stirred for 2 hr at room temperature. The sample was clarified by centrifugation and the supernatant was incubated overnight at ambient temperature with Ni-NTA agarose resin beads (Macherey-Nagel, Düren, Germany) equilibrated with 20 mM Tris pH 8.0, 250 mM NaCl, 10 mM imidazole, 6 M urea, and 1 mM DTT. Immobilized protein was refolded on-column with a linear gradient of 6 to 0 M urea and 1 to 0 mM DTT and eluted with elution buffer (containing 500 mM imidazole) followed by dialysis and overnight TEV-protease cleavage. AETX-K was separated from this mixture by reverse-phase HPLC on a C18 column using an H_2O:MeCN gradient, lyophilized and kept at −20 °C for storage. For expression of ^{2}H,^{15}N-labeled AETX-K for binding to LPN-channels, after initially inoculating an M9 culture and growing to OD_{600}~0.5, cells were transferred to $^{2}H_2O$-based M9 medium supplemented with 2 g/L d_7-glucose and 0.5 g/L DN-IsoGro powder (Sigma-Aldrich).

2.3 | Preparation of LPN-channel assemblies

The KcsA channel (residues 16–160) and chimeric Kv1.1 channel (Supplemental Figure S1) were overexpressed in C41 *E. coli* bacteria and purified without isotopic labeling following previously described procedures (18). For optimal yields the extraction buffer contained 1.5% w/v *n*-dodecyl-N,N-dimethyl-3-ammonio-1-propanesulfonate (Anzergent 3–12) and 1.2 M KCl. The final buffer for elution from the Ni^{2+}-affinity column contained 5 mM dodecyl maltoside (DDM). Full-length membrane scaffold protein was expressed in BL21(DE3) *Escherichia coli* transformed with a pET28a plasmid encoding for MSP1D1 fused to a tobacco etch virus (TEV) protease cleavage site and containing an N-terminal His_6 tag. Overexpression and purification were performed as previously described (19), with final dialysis performed against 20 mM Tris pH 7.5, 100 mM NaCl, 0.5 mM EDTA) in preparation for incorporation into LPNs. A 3-to-1 mol:mol mixture of 1-palmitoyl-2-oleoyl-*sn*-glycero-3-phosphocholine:1-palmitoyl-2-oleoyl-*sn*-glycero-3-phospho-*rac*-glycerol (POPC:POPG) was solubilized in MeOH:$CHCl_3$ (35:65) and lyophilized. The channel sample was mixed with MSP1D1, lipids, and sodium cholate at 1:20:800:1600 molar ratio, while maintaining a final cholate concentration of 12–40 mM and incubated overnight with moderate shaking at 25 °C. SM-2 BioBeads (BioRad, 0.5 gr per 1mL of assembly mixture) were then added, and shaking was continued for 2 h. After removal of the BioBeads the LPN-channel assembly was purified on a Ni^{2+} affinity column equilibrated in 20 mM Tris pH 7.5, 100 mM NaCl, 20 mM imidazole buffer, and the protein-containing LPNs were eluted by addition of 500 mM imidazole. The eluted channel-containing nanodiscs were concentrated and purified on a Superdex200 16/60 size exclusion column (GE Healthcare, Uppsala, Sweden) equilibrated with 20 mM Tris pH 7.5, 100 mM NaCl, 0.5 mM EDTA, concentrated, and preserved at 4 °C until use.

2.4 | Two Electrode Voltage Clamp (TEVC)

Xenopus laevis oocytes consistent with stage VI were selected based on their size and clear white equatorial bands and were injected with 0.05 ng of cRNA encoding Kv1.1, Kv1.1-L_{296}F, or other Kv channels. Recording solution was (in mM): 4 KCl, 100 NaCl, 1 $MgCl_2$, 0.3 $CaCl_2$, 10 HEPES, pH 7.5. Recordings were performed with constant gravity flow of solution at 2 mL/min, yielding chamber exchange in 5 s. Currents were recorded 2 days after cRNA injection using an Oocyte clamp amplifier OC-725C (Warner Instruments)

and electrodes filled with 3 M KCl with resistance of 0.3–1 MΩ. Data were filtered at 1 kHz and digitized at 20 kHz using pClamp software and assessed with Clampfit v9.0 and Origin 6.0. Equilibrium inhibition of AETX-K was determined by fitting the concentration-response curve, whereas it was calculated for AETX-K variants from the fraction of unblocked current achieved by one to three toxin concentrations that inhibited 20–80% of the current, as described before (10). K_{on} and K_{off} were estimated from fits of the kinetics of toxins wash-in and wash-off. Thus, according to a bimolecular scheme with a single toxin-bound state and changes in toxin concentration compared to the speed of block and unblock, one can assess steady-state and kinetic parameters of blockade. The unblocked fractional current at equilibrium (F_{un}) with a toxin concentration [Tx] relates to the concentration dependence of inhibition according to Hill equation: $F_{un} = (1 + [Tx]/K_i)^{-1}$, where F_{un} is related to the second-order association rate constant $K_{on}(1/Ms)$ and first-order dissociation rate constant $K_{off}(1/s)$ according to equation: $F_{un} = K_{off}/(K_{on}[Tx] + K_{off})$, and the equilibrium inhibition constant for half-maximal blockade K_i is given by the equation: $K_i = K_{off}/K_{on}$. Time constants of block and unblock (τ_{on} and τ_{off}) were determined by single exponential fits of the kinetics of toxin wash-in and wash-off, and these parameters are related to K_{on} and K_{off} by equations: $\tau_{on} = (K_{on}[Tx] + K_{off})^{-1}$ and $\tau_{off} = (K_{off})^{-1}$. The G-V relationships were fitted to the Boltzmann equation: $G = G_{max}/[1 + \exp(-zF(V-V_{1/2})/RT)]$, where G_{max} is maximum conductance, V is the test potential, $V_{1/2}$ is the voltage of half-maximal activation, z is the effective valence, T is the temperature, R is the gas constant, and F is the Faraday constant. The theoretical percentages of expression of the five different stoichiometries of assembled channels of Kv1.1-Kv1.2 were calculated with the binomial equation $F_i = \{4!/[(4-n)!n!]\} F_{kv1.1}^{(4-n)} F_{kv1.2}^{n}$, where F_i is the decimal fraction of channels with n Kv1.2 subunits, $F_{Kv1.1}$ is the fraction of Kv1.1 cRNA injected, and $F_{Kv1.2}$ is the fraction of Kv1.2 cRNA injected, both $F_{Kv1.1}$ and $F_{Kv1.2}$ are 0.5 in this study. For Kv1.1-Kv1.2 channels, n ranges from 0 to 4, giving five channel types based on subunit composition (Figure 7E).

2.5 | NMR sample preparation

Lyophilized synthetic or recombinant labeled AETX-K were dissolved in 20 mM phosphate buffer (pH 6.8) containing 10 mM NaCl, 0.02% NaN_3 and 7% ^2H_2O. Typical AETX-K and HmK D14Q concentrations were 300–1000 μM for assignment and structure determination experiments and 50 μM ^2H,^{15}N-AETX-K for LPN-channel binding experiments. For the latter LPN-channel was titrated in from a stock solution of 150-200 μM of tetrameric channel to reach the desired toxin:channel ratio.

2.6 | NMR spectroscopy and structure determination

All NMR measurements were performed with a Bruker DRX 700 spectrometer equipped with a cryogenic triple-resonance TCI probe and z-axis pulsed field gradients at 16.4 T and 298 K (structure determination) or 303 K (LPN-channel binding). Chemical shifts were directly referenced against 4,4-dimethyl-4-sila-pentane-1-sulfonic acid (DSS) present at ~1 mM. All spectra were processed by using the TopSpin 3.5 package (Bruker BioSpin, Karlsruhe, Germany). Assignments of AETX-K ^1H chemical shifts were obtained from homonuclear 2D total correlation spectroscopy (TOCSY) and 2D nuclear Overhauser effect

spectroscopy (NOESY) spectra. An ^{15}N-edited 3D-NOESY spectrum served to assign ambiguous ^{1}H shifts as well as the ^{15}N shifts. Assignments of ^{13}Cα/^{13}Cβ shifts were obtained from a 2D ^{1}H,^{13}C-HMQC spectrum by comparison to known ^{1}H shifts. Details of NMR acquisition parameters are summarized in the Supplementary Information.

For structure determination NOESY cross peaks from 2D- and 3D-spectra were assigned, normalized for multiplicity and binned by intensity into strong, medium, weak and very weak groups, and these were assigned ^{1}H-^{1}H distances of 2.5, 3.3, 4.0 and 5.0 Å, respectively. Appropriate distance constraints were employed with a +30% tolerance. TALOS+ predictions for backbone ϕ/ψ dihedral angles were added as dihedral constraints with a tolerance of ±30°. The CNS1.3 structure calculation suite was employed with these constraints as input to determine 81 accepted structures, of which 23 low-energy structures were chosen for the final ensemble.

3 | RESULTS

3.1 | AETX-K blocks Kv1.1 potently and specifically

AETX-K was identified in the Sea anemone *Anemonia erythraea* (20). AETX-K has 34 residues, including six cysteine residues that form three intramolecular disulfide bonds with Cys2–Cys34, Cys11–Cys27, and Cys16–Cys31 (Figure 1A) to yield the distinct SAK1 scaffold. SAK1 toxins block Kv channels similarly to α-KTx scorpion toxins via binding to the external pore vestibule and occlusion of the conduction pore by a positively charged residue (9, 14). Thus, HmK blocks using Lys_{22}, whereas Hui1 and ShK uses a non-classical residue two position further across the toxin interaction surface, Hui1-Arg_{23}/ShK-Arg_{24} (10, 12). AETX-K shares 67% identity to HmK in primary sequence and 88% identity to Hui1 (Figure 1A).

cRNA encoding Kv1.1 was synthesized *in vitro* and injected into *Xenopus* oocytes, yielding robust outward K^+ currents that were recorded using two-electrode voltage clamp (TEVC) two days after injection. Incubation with 50 pM AETX-K inhibited ~96% of K^+ currents at 0 mV (Figure 2A). AETX-K blocked Kv1.1 reversibly with association and dissociation constants of $K_{on} = 1.7 \times 10^9 \pm 0.2 \times 10^9$ /M·s and $K_{off} = 2.3 \times 10^{-3} \pm 0.3 \times 10^{-3}$ /s, respectively, determined by single-exponential fits to the time courses for block and unblock on acute application and washout of AETX-K (Figure 2B). AETX-K inhibited Kv1.1 currents in a dose-dependent manner. A fit of the dose–response at 0 mV with the Hill equation (Materials and Methods) yielded a $K_i = 1.6 \pm 0.2$ pM and a Hill coefficient of 1.03 ± 0.21, consistent with an expected mechanism of block of the channel by one peptide on the pore (Figure 2C).

AETX-K was found to be quite specific for Kv1.1. Kv1.2 is another Kv channel in the Kv1 subfamily that is prominently expressed in the central nervous system (21). Kv1.1 and Kv1.2 share the same topology and 80% identity in their primary sequences. AETX-K blocks Kv1.2 with an estimated K_i of 2.2 μM (Table 1), that is, ~1.4 million-fold less well than it blocks Kv1.1. Kv1.3 channels are expressed in various cell types in the brain, muscle, and leucocytes, and are blocked by many venom-derived peptides (22). AETX-K blocks Kv1.3 with an estimated K_i of 1.2 μM (Table 1), ~800,000-fold less well than Kv1.1. Further, 10

μM AETX-K showed no inhibition of Kv1.5, a channel expressed in the human heart, brain, and pancreatic cells (23). Nor did 10 μM AETX-K inhibit homotetrameric channels formed by Kv7.2 or heterotetrameric channels formed by Kv7.2 and Kv7.3 (M-channels) (Table 1) that are expressed in the brain and linked to a spectrum of seizure disorders (24). In contrast, HmK tested on this panel of channels was again observed to be promiscuous, blocking all the K^+ channels with K_i from 75 pM to 9.8 μM (Table 1).

3.2 | The NMR structure of AETX-K

To assess the structural basis for toxin inhibition, the three-dimensional structure of AETX-K was determined using standard 2D- and 3D-NMR methods (Materials and Methods). ^{15}N-labeled AETX-K was expressed heterologously and purified by fast protein liquid chromatography (FPLC) and high-performance liquid chromatography (HPLC) (Materials and Methods) (25). A total of 297 proton-proton distance and 43 TALOS-based (26) dihedral angle constraints were employed to derive an ensemble of 23 low energy structures exhibiting a backbone (all heavy atoms) root mean square deviation (rmsd) of 0.47 (1.24) Å (Table S1, PDB accession code 7OD2). AETX-K residues Thr_{12}-Thr_{18} and Met_{20}-Thr_{26} adopt tight α-helical conformations as part of the typical SAK1 helix-kink-helix structure constrained by the Cys_{11}-Cys_{27} and Cys_{16}-Cys_{31} disulfide bonds (Figure 3A). As expected for this family of homologous toxins, the overall fold and orientation of sidechains Lys_{21} and Lys_{23} are quite similar to that of HmK (Figure 3B) (12), and Hui1 (PDB 2N6B) (10). However, comparing surface electrostatic maps for AETX-K and HmK reveals a striking difference. Similar to Hui1, AETX-K presents a uniformly positively charged surface, including contributions from residues Lys_8, Arg_{15}, Arg_{17}, Lys_{21}, Lys_{23} (Arg_{23} in Hui1), and Lys_{28}. In both toxins the single acidic residue, Asp_4, is involved in a structure-stabilizing salt bridge with residue Lys_{29}. In contrast, the N-terminal region of HmK is less positively charged because of two amino acid substitutions in this region, Lys_8/Val_9, and Gln_{13}/Asp_{14}, resulting in a channel-binding surface with very different electrostatic properties (Figure 3B).

To study the interaction between AETX-K and the Kv1.1 channel by high-resolution NMR methods we embedded tetramers of the Kv1.1 pore as a chimera in KcsA backbone or KcsA in lipoprotein nanodiscs (LPNs) stabilized by a membrane scaffolding protein (19, 27). To create the chimeric protein with Kv1.1 pore, we replaced 13 residues in the turret region and 2 residues in the extracellular pore vestibule region of KcsA where SAK1 toxins usually bind (10, 28), with the homologous residues in Kv1.1 (Supplemental Figure S1). Suggesting AETX-K binds to KcsA and the Kv1.1 pore chimera directly, adding sub-stoichiometric concentration of the channels into a ^{2}H,^{15}N-labeled AETX-K sample resulted in a loss of cross-peak intensity in the fingerprint ^{1}H,^{15}N-HSQC spectrum of AETX-K (Figure 4A). Due to the large size of the LPN-channel assembly, estimated at 150 kDa, signal loss in these experiments is a combination of immobilization of the toxin and exchange broadening, both induced by formation of the toxin-channel complex. Observing a weakening (rather than shifting) of peaks is a hallmark of strong binding to the channel, reflecting slow exchange on the NMR timescale between free and bound forms of AETX-K. Thus, at 0.33:1.0 mol:mol channel:AETX-K, the reduction of intensity reduction was considerably more for the Kv1.1 chimera (66 ± 4%) than KcsA (25 ± 9%) (Figure 4), consistent with a

stronger interaction with the Kv1.1 channel turret and extracellular pore vestibule regions. Notably, when focusing on the central helix-kink-helix motif of the AETX-K toxin (residues Gln_{13}-Thr_{26}), the intensity loss is above average, 74% and 34% for the Kv1.1 chimera and KcsA, respectively (Figure 4B). This is an indication that residues in this region are, as anticipated from the current view of the toxin-channel interface, intimately involved in the interaction with the channel. These findings are also consistent with our findings that AETX-K blocks the Kv1.1 and KcsA pore with affinities of 1.6 pM and 0.3 nM (10), respectively.

3.3 | AETX-K occludes the Kv1.1 pore via Lys_{23}

AETX-K blockade of Kv1.1 follows expectations for a pore-directed toxin inhibitor whereby one molecule occludes the channel conduction pathway. Thus, the dose–response for AETX-K inhibition of Kv1.1 showed a Hill coefficient of ~1 (Figure 2C) and fits to the time courses for AETX-K association and dissociation were single-exponential (Figure 2B), as expected for a simple biomolecular interaction relaxing to equilibrium (10).

We previously studied the blocking mechanism of HmK, Hui1 and ShK, showing that HmK, Hui1 and ShK blockade are sensitive to voltage, and this depends on their positively charged residues HmK-Lys_{22}, Hui1-Arg_{23}, and ShK-Arg_{24} respectively, interacting with K^+ traversing the pore from the intracellular compartment (Figure 1B) (10, 12). Like HmK, Hui1 and ShK, the dissociation rate of AETX-K from Kv1.1 was sensitive to voltage (Figure 5A). To confirm the blocking mechanism of AETX-K, we first neutralized the residue corresponding to HmK-Lys_{22} in AETX-K to produce AETX-K-K_{21}N. AETX-K-K_{21}N diminished toxin inhibition, showing an attenuation of ~1.1 million-fold (Table 2); however, neutralization of AETX-K-K_{21} did not affect the voltage dependence of toxin dissociation (Figure 5B). We next neutralized the residue corresponding to Hui1-Arg_{23} in AETX-K to produce AETX-K-K_{23}N. AETX-K-K_{23}N only attenuated the K_i ~ 0.1 million-fold (Table 2); however, the mutation eliminated the voltage dependence of toxin dissociation (Figure 5B). Thus AETX-K Lys_{23}, not Lys_{21}, mediated the voltage dependence of toxin dissociation consistent with the Lys in the non-classical position (homologous to Hui-Arg_{23} and ShK-Arg_{24}) occluding the Kv1.1 pore.

3.4 | AETX-K blocks the gain-of-function channel Kv1.1-L_{296}F

The mutant channel Kv1.1-L_{296}F alters a residue in the voltage sensor that moves to open the channel pore (S5-S6) (Figure 1B) (5). Injecting the same amount of cRNA encoding Kv1.1-L_{296}F into *Xenopus* oocytes as for WT Kv1.1 channels produced larger peak outward K^+ currents and slower closure on return to the resting potential compared to WT (Figure 6A). At 0 mV, the current amplitude of Kv1.1-L_{296}F was ~ 3.1-fold larger than WT (Figure 6A and 6D). This was explained by a shift in the half-maximal ($V_{1/2}$) conductance-voltage (G-V) relationship of −59 mV for Kv1.1-L_{296}F compared to WT, favoring opening of the mutant channel at potentials where the WT is closed (Figure 6B). A fit of the dose–response curve for inhibition by AETX-K at 0 mV yielded a K_i = 2.1 ± 0.1 pM and a Hill coefficient of 1.02 ± 0.03 (Figure 6C). Incubation with 4 pM AETX-K reduced Kv1.1-L_{296}F currents ~ 3.1-fold at 0 mV, bringing the current-voltage (I-V) relationship of Kv1.1-L_{296}F to a comparable level of that for uninhibited WT channels (Figure 6D). Finally, AETX-K

binding did not change the voltage-dependence of activation of the channels (Supplemental Figure S2). Thus, the peptide blocks the gain of function channel effectively showing only ~1.3-fold loss of affinity compared to WT channels, presumably due to increased "knock-off" with increased open probability rather than a change in the pore binding site per se, and this is easily offset by applying 2.1 pM rather than 1.6 pM to achieve half-block at 0 mV.

3.5 | AETX-K blocks Kv1.1-Kv1.2 heterotetrameric channels

Kv1.1 subunits can form homotetrameric channels or heterotetrameric channels with other Kv1 subunits in vivo (3, 4). Kv1.2 is the predominant subunit that forms heterotetrameric channels with Kv1.1 in neuronal membranes (3). Both Kv1.1 and Kv1.2 are voltage gated and open at negative membrane potentials with a $V_{1/2}$ of −23 mV and −5 mV, respectively (Figure 7A and B). We note above that Kv1.2 channels are over a million-fold less sensitive to AETX-K (K_i ~ 2.2 μM) than Kv1.1, suggesting that the peptide might inhibit mixed channel complexes poorly; however, incorporation of Kv1.2 subunits suppresses AETX-K in a recessive manner. To study the blockade of Kv1.1-Kv1.2 heterotetrameric channels, we combined cRNAs encoding Kv1.1 and Kv1.2, in a 1:1 ratio and injected the mixture into *Xenopus* oocytes. Assuming unbiased assembly, channels will form with four subunits and various ratios of the two subunits according to a binomial distribution as for other Kv channels (29), 6% with four Kv1.1 ($Kv1.1_4$), 25% with three Kv1.1 ($Kv1.1_3$-Kv1.2), 38% with two Kv1.1 ($Kv1.1_2$-$Kv1.2_2$), 25% with one Kv1.1 (Kv1.1-$Kv1.2_3$) and 6% with no Kv1.1 ($Kv1.2_4$) (Figure 7C). The composite behavior of the channels yielded a current amplitude smaller than Kv1.1 and bigger than Kv1.2, with an apparent $V_{1/2}$ of −14 mV (Figure 7A and B). Whereas 100 pM AETX-K fully blocked Kv1.1 channels and did not block on Kv1.2 channels, the mixed population was blocked ~22% (Figure 7D-E). Application of 10 nM AETX-K blocked the population by 47% and 1000 nM by 82% (Figure 7F). One can estimate the relative affinity of AETX-K for the $Kv1.1_3$-Kv1.2 channels by assuming that 100 pM fully blocks $Kv1.1_4$ and 64% of $Kv1.1_3$-Kv1.2 channels, giving an estimated K_i of 56 pM according to Hill equation (see detailed calculation in Table 3). Similarly, the K_i for $Kv1.1_2$-$Kv1.2_2$ and Kv1.1-$Kv1.2_3$ can be estimated to be ~14 nM and 1155 nM (Table 3). Based on these estimates and the Hill equation, we anticipated the percentage of block of the mixed population K^+ currents to be 67% when 100 nM AETX-K was applied, similar to the 68% blockade we observed (Figure 7F), supporting the estimated affinities.

4 | DISCUSSION

4.1 | AETX-K is a potent and specific blocker of Kv1.1

Kv1.1 can be blocked by several small molecules. Tetraethylammonium (TEA) is widely used to study K^+ channels and inhibits Kv1.1 channels with an affinity of 0.4 mM by binding to Kv1.1-Tyr_{379} in the extracellular pore vestibule (30). Another well-known small molecule blocker of Kv1.1 is 4-AP (31), which blocks Kv1.1 with an affinity of 17 μM by crossing the plasma membrane to bind to the intracellular vestibule of the channel (5). 4-AP has been shown to be effective in clinical trials in patients with downbeat nystagmus, episodic ataxia type 2, and multiple sclerosis (32), although it has proven to be toxic

for some patients, causing neurologic excitability, gastrointestinal effects, diaphoresis, and cardiac toxicity (7). Two other major disadvantages of these small molecule blockers are their lack of potency and specificity. TEA and 4-AP block many K^+ channels with an affinity range from μM to mM because they interact only with a few channel residues, usually at conserved motifs. In contrast, venom-derived peptides can provide higher affinity and specificity than small molecules because of their larger interaction surface with the channels. Compared to other known Kv1.1 peptide blockers, AETX-K affinity is many orders more avid at K_i ~ 1.6 pM and shows ~1.4-million-fold and ~760,000-fold greater selectivity over Kv1.2 and Kv1.3, respectively (Table 1). Thus, the scorpion venom toxin KTx blocks Kv1.1 with K_i ~ 1 nM but also blocks Kv1.1, Kv1.2, Kv1.3 and BK channels at nM level (33, 34). Dendrotoxin-K (DTX-K) from the mamba snake venom blocks both Kv1.1 and Kv1.2 with K_i ~ 0.6 nM and ~ 9.6 nM, respectively (35, 36). Other well studied SAK1 toxins, such as ShK and BgK, block Kv1.1, Kv1.2, and Kv1.3 almost equally well (Table S2) (9).

4.2 | AETX-K blocks Kv1.1 via a Lys in an unexpected location

An effective drug should bind with high specificity to its intended target to avoid the risk of deleterious side effects. AETX-K has striking specificity for Kv1.1 compared to other peptide toxins that we suspect is conferred by occlusion of the pore via a classical residue, lysine, located in an unexpected location. We have previously described two blocking mechanisms for SAKI toxins. We observed HmK to interact with trans-ions passing through KcsA and Kv1.3 via Lys_{22}, a residue in a classical location on the toxin interaction surface homologous to the conserved blocking lysine in α-KTx scorpion toxins such as CTX-Lys_{27} (12). In contrast, we have also found that the chimeric SAK1 toxin Hui1 and the natural toxin ShK blocked KcsA and Kv1.3 using an arginine residue, Hui1-Arg_{23} and ShK-Arg_{24}, respectively, two positions past the canonical blocking lysine, indicative of an alternative binding orientation (10). Here we show that AETX-K deploys Lys_{23} (and not Lys_{21}) to inhibit the Kv1.1 pore, adopting the Hui1 and ShK-like Arg-mediated blocking mechanism. We surmise AETX-K blocks Kv1.1-Kv1.2 channels with the same binding orientation since the toxins we have studied to-date have been consistent in their binding orientation independently of channel type; for example, HmK blocks both KcsA and Kv1.3 pores using its Lys_{22} (12).

Our NMR chemical shift perturbation experiments (Figure 4) confirm the helix-kink-helix region where AETX-K-Lys_{23} is located to be embedded near the channel pore and studies of the voltage dependence of dissociation of AETX-K charge variants establish that it blocks Kv1.1 via Lys_{23}, the residue is located where Hui1 deploys Arg_{23} to block (Figure 5). Like AETX-K, Hui1 manifests notable specificity (10) suggesting the alternative binding strategy may not be available in all channels. Supporting this notion, the relative positions of the classical site (AETX-K-Lys_{21}) and non-classical site (AETX-K-Lys_{23}) are on opposite faces of the second helix with their side chains offset by ~150° in the various low-energy structures (Figure 3). This implies that the binding orientations for AETX-K/Hui1 versus HmK vary by a significant rotation around the long axis of the toxins and therefore may involve quite different contacts in the turret region and the extracellular pore vestibule of the channels allowing for interaction with residues that are not conserved in other K^+ channels.

These findings are consistent with reports that changing the charged residues on a scorpion toxin altered the orientation of binding in Kv1.3 (37). Accordingly, we surmise that the contrasting electrostatic surface potentials of Hui/AETX-K and HmK contribute to their differing binding orientations. Of course, the binding interface of the Kv1.1 channel, which exhibits a net –5 charge across the extracellular loops that form the outer vestibule, also contributes to the structure of the complex. Of note, our finding that SAK1 blocks Kv1.3 by an Arg-dependent non-classical mechanism like Hui1 (12), suggests that the model of ShK with Kv1.3 that assumed Lys_{22} to be in the pore may need to be revisited (38).

A crystal structure of the scorpion toxin CTX in complex with a homomeric Kv1.2 channel (16) demonstrated how the toxin interaction surface residues inferred by mutational studies (13, 14) interact with the channel. Thus, CTX-Lys_{27} (homologous to AETX-K-Lys_{23}) that mediates trans-ion "knock-off" inserts into the selective filter forming hydrogen-bonds with the carbonyl backbone at Kv1.2-Y_{377} on the four subunits. Other functional toxin residues on the interaction surface (CTX-M_{29},CTX-Y_{36}, CTX-R_{25} and CTX-R_{34}) were shown to pack against Kv1.2-D_{379} and Kv1.2-V_{381}, or to interact electrostatically with Kv1.2-D_{363} in the pore helix and Kv1.2-Q_{357} in the pre-helix turret region (Supplemental Figure S3) (16). Given the similarity of the Kv1.1 and Kv1.2 pore residues, and that AETX-K has similar hydrophobic and basic residues like CTX surrounding the key AETX-K-Lys_{23} which mediates the trans-ion effect, we suspect the toxin will have contacts in Kv1.1 and Kv1.2 at the conserved residues noted above in the CTX-Kv1.2 structure including Kv1.2-Y_{377}, Kv1.2-D_{379}, Kv1.2-V_{381} in and near the selectivity filter and perhaps Kv1.2-D_{363} in the pore helix as well as turret sites.

4.3 | AETX-K may offer a strategy to treat diseases caused by Kv1.1 hyperactivity

Studies of Kv1.1 knockout (KO) mice and isolated hippocampal neurons showed that loss of Kv1.1 in the hippocampus can underlie seizure generation (1, 2). The Kv1.1 KO mice show premature death, develop temporal lobe epilepsy spontaneously, exhibit cardio-respiratory failure, and experience sudden death (1, 2). Moreover, loss-of-function mutations in the human Kv1.1 gene have been linked to ataxia, myokymia, and epilepsy (1, 39). In recent years, diseases caused by Kv1.1 hyperactivity have been reported. For instance, Kv1.1 was found to overexpress outside the nodes of Ranvier in demyelinated axons of optic nerve, and blocking the channel with 100 nM DTX_K ameliorated multiple sclerosis-related symptoms in mice (4). In addition, gain-of-function mutations of Kv1.1 have been reported, including the drug-resistant Kv1.1-L_{296}F mutation in the VSD we consider here as well as a Kv1.1-A_{261}T mutation in the S3 transmembrane segment that causes mild, drug-responsive, focal epilepsy in patients (8). Recently, gain-of-function mutations of Kv1.6 were found to be associated with neurodevelopmental disorders and seizures in patients (40). Because Kv1.6 and Kv1.1 share high similarity in the pore region (Supplemental Figure S3) and form heterotetrametric channels in the human brain, AETX-K is anticipated to suppress excess current passed by these gain-of-function channels as well. The increased K^+ currents likely lead to excess repolarization, and action potential shortening, disrupting the firing frequency and dampening neuronal excitability (1). Although 4-AP showed beneficial effects in treating a patient with Kv1.1 gain-of-function mutation-associated epilepsy (5), it has been reported to produce side effects (7). AETX-K, a peptide with ~ 10-million-fold better

affinity and superior specificity compared to 4-AP may serve as a lead for an alternative therapeutic strategy. In recent years, significant progress has been made using peptide biologics to diagnose and treat various diseases (41). Peptide therapeutics have improved in part because they are amenable to structural modification to influence pharmacodynamics and pharmacokinetics and formulations can be varied for delivery. Thus, the disadvantages of many unmodified peptides for use as drugs, like short half-life and rapid elimination from the body, have been confronted by chemical modifications, cyclization, unnatural amino acid substitutions, high molecular weight polyethyleneglycol (PEG) conjugation, and alternative delivery systems (41). Moreover, the intramolecular disulfide bonds in venom-derived peptides like AETX-K provide excellent thermal and proteolytic stability. Although intrathecal administration is has been favored for venom-derived peptide therapy targeting the central nervous system (42), they do cross the blood-brain barrier via passive diffusion or saturable transport pathways after intraperitoneal or intravenous injection (43, 44) or using designed drug carriers (45). To date, 15 therapeutic peptides have been approved for clinical use, and several other peptide candidates are undergoing clinical trials (41).

Supplementary Material

Refer to Web version on PubMed Central for supplementary material.

ACKNOWLEDGMENTS

This work was supported by NIH [GM111716 to SANG., HL159711 to SANG. and RZ, AT012544 to RZ and SANG, and the US–Israel Binational Science Foundation (BSF 2017243) to SANG and JC.

DATA AVAILABILITY STATEMENT

All data needed to evaluate the conclusions in the paper are presented in the paper.

REFERENCES

1. D’Adamo MC, Liantonio A, Rolland JF, Pessia M, and Imbrici P (2020) Kv1.1 Channelopathies: Pathophysiological Mechanisms and Therapeutic Approaches. Int J Mol Sci 21
2. Smart SL, Lopantsev V, Zhang CL, Robbins CA, Wang H, Chiu SY, Schwartzkroin PA, Messing A, and Tempel BL (1998) Deletion of the K(V)1.1 potassium channel causes epilepsy in mice. Neuron 20, 809–819 [PubMed: 9581771]
3. Ovsepian SV, LeBerre M, Steuber V, O’Leary VB, Leibold C, and Oliver Dolly J (2016) Distinctive role of KV1.1 subunit in the biology and functions of low threshold K(+) channels with implications for neurological disease. Pharmacol Ther 159, 93–101 [PubMed: 26825872]
4. Bagchi B, Al-Sabi A, Kaza S, Scholz D, O’Leary VB, Dolly JO, and Ovsepian SV (2014) Disruption of myelin leads to ectopic expression of K(V)1.1 channels with abnormal conductivity of optic nerve axons in a cuprizone-induced model of demyelination. PLoS One 9, e87736 [PubMed: 24498366]
5. Muller P, Takacs DS, Hedrich UBS, Coorg R, Masters L, Glinton KE, Dai H, Cokley JA, Riviello JJ, Lerche H, and Cooper EC (2023) KCNA1 gain-of-function epileptic encephalopathy treated with 4-aminopyridine. Ann Clin Transl Neurol 10, 656–663 [PubMed: 36793218]
6. Judge SI, and Bever CT Jr. (2006) Potassium channel blockers in multiple sclerosis: neuronal Kv channels and effects of symptomatic treatment. Pharmacol Ther 111, 224–259 [PubMed: 16472864]
7. King AM, Menke NB, Katz KD, and Pizon AF (2012) 4-aminopyridine toxicity: a case report and review of the literature. J Med Toxicol 8, 314–321 [PubMed: 22782458]

8. Miceli F, Guerrini R, Nappi M, Soldovieri MV, Cellini E, Gurnett CA, Parmeggiani L, Mei D, and Taglialatela M (2022) Distinct epilepsy phenotypes and response to drugs in KCNA1 gain- and loss-of function variants. Epilepsia 63, e7–e14 [PubMed: 34778950]

9. Diochot S, and Lazdunski M (2009) Sea anemone toxins affecting potassium channels. Prog Mol Subcell Biol 46, 99–122 [PubMed: 19184586]

10. Zhao R, Dai H, Mendelman N, Cuello LG, Chill JH, and Goldstein SA (2015) Designer and natural peptide toxin blockers of the KcsA potassium channel identified by phage display. Proc Natl Acad Sci U S A 112, E7013–7021 [PubMed: 26627718]

11. Doyle DA, Morais Cabral J, Pfuetzner RA, Kuo A, Gulbis JM, Cohen SL, Chait BT, and MacKinnon R (1998) The structure of the potassium channel: molecular basis of K+ conduction and selectivity. Science 280, 69–77 [PubMed: 9525859]

12. Zhao R, Dai H, Mendelman N, Chill JH, and Goldstein SAN (2020) Tethered peptide neurotoxins display two blocking mechanisms in the K(+) channel pore as do their untethered analogs. Sci Adv 6, eaaz3439 [PubMed: 32181366]

13. MacKinnon R, and Miller C (1988) Mechanism of charybdotoxin block of the high-conductance, Ca2+-activated K+ channel. J Gen Physiol 91, 335–349 [PubMed: 2454283]

14. Goldstein SA, Pheasant DJ, and Miller C (1994) The charybdotoxin receptor of a Shaker K+ channel: peptide and channel residues mediating molecular recognition. Neuron 12, 1377–1388 [PubMed: 7516689]

15. Miller C (1995) The charybdotoxin family of K+ channel-blocking peptides. Neuron 15, 5–10 [PubMed: 7542463]

16. Banerjee A, Lee A, Campbell E, and Mackinnon R (2013) Structure of a pore-blocking toxin in complex with a eukaryotic voltage-dependent K(+) channel. Elife 2, e00594 [PubMed: 23705070]

17. Chang SC, Galea CA, Leung EW, Tajhya RB, Beeton C, Pennington MW, and Norton RS (2012) Expression and isotopic labelling of the potassium channel blocker ShK toxin as a thioredoxin fusion protein in bacteria. Toxicon 60, 840–850 [PubMed: 22659540]

18. Chill JH, Louis JM, Miller C, and Bax A (2006) NMR study of the tetrameric KcsA potassium channel in detergent micelles. Protein Sci 15, 684–698 [PubMed: 16522799]

19. Hagn F, Nasr ML, and Wagner G (2018) Assembly of phospholipid nanodiscs of controlled size for structural studies of membrane proteins by NMR. Nat Protoc 13, 79–98 [PubMed: 29215632]

20. Hasegawa Y, Honma T, Nagai H, Ishida M, Nagashima Y, and Shiomi K (2006) Isolation and cDNA cloning of a potassium channel peptide toxin from the sea anemone Anemonia erythraea. Toxicon 48, 536–542 [PubMed: 16905168]

21. Robbins CA, and Tempel BL (2012) Kv1.1 and Kv1.2: similar channels, different seizure models. Epilepsia 53 Suppl 1, 134–141

22. Wulff H, and Pennington M (2007) Targeting effector memory T-cells with Kv1.3 blockers. Curr Opin Drug Discov Devel 10, 438–445

23. Borrego J, Feher A, Jost N, Panyi G, Varga Z, and Papp F (2021) Peptide Inhibitors of Kv1.5: An Option for the Treatment of Atrial Fibrillation. Pharmaceuticals (Basel) 14

24. Abbott GW (2020) KCNQs: Ligand- and Voltage-Gated Potassium Channels. Front Physiol 11, 583 [PubMed: 32655402]

25. Sher I, Chang SC, Li Y, Chhabra S, Palmer AG 3rd, Norton RS, and Chill JH (2014) Conformational flexibility in the binding surface of the potassium channel blocker ShK. Chembiochem 15, 2402–2410 [PubMed: 25236806]

26. Shen Y, Delaglio F, Cornilescu G, and Bax A (2009) TALOS+: a hybrid method for predicting protein backbone torsion angles from NMR chemical shifts. J Biomol NMR 44, 213–223 [PubMed: 19548092]

27. Denisov IG, Grinkova YV, Lazarides AA, and Sligar SG (2004) Directed self-assembly of monodisperse phospholipid bilayer Nanodiscs with controlled size. J Am Chem Soc 126, 3477–3487 [PubMed: 15025475]

28. Selvakumar P, Fernandez-Marino AI, Khanra N, He C, Paquette AJ, Wang B, Huang R, Smider VV, Rice WJ, Swartz KJ, and Meyerson JR (2022) Structures of the T cell potassium channel Kv1.3 with immunoglobulin modulators. Nat Commun 13, 3854 [PubMed: 35788586]

29. MacKinnon R (1991) Determination of the subunit stoichiometry of a voltage-activated potassium channel. Nature 350, 232–235 [PubMed: 1706481]
30. Bretschneider F, Wrisch A, Lehmann-Horn F, and Grissmer S (1999) External tetraethylammonium as a molecular caliper for sensing the shape of the outer vestibule of potassium channels. Biophys J 76, 2351–2360 [PubMed: 10233054]
31. Stephens GJ, Garratt JC, Robertson B, and Owen DG (1994) On the mechanism of 4-aminopyridine action on the cloned mouse brain potassium channel mKv1.1. J Physiol 477, 187–196 [PubMed: 7932213]
32. Dietrich M, Hartung HP, and Albrecht P (2021) Neuroprotective Properties of 4-Aminopyridine. Neurol Neuroimmunol Neuroinflamm 8
33. Kourrich S, Mourre C, and Soumireu-Mourat B (2001) Kaliotoxin, a Kv1.1 and Kv1.3 channel blocker, improves associative learning in rats. Behav Brain Res 120, 35–46 [PubMed: 11173083]
34. Takacs Z, Toups M, Kollewe A, Johnson E, Cuello LG, Driessens G, Biancalana M, Koide A, Ponte CG, Perozo E, Gajewski TF, Suarez-Kurtz G, Koide S, and Goldstein SA (2009) A designer ligand specific for Kv1.3 channels from a scorpion neurotoxin-based library. Proc Natl Acad Sci U S A 106, 22211–22216 [PubMed: 20007782]
35. Chi XX, and Nicol GD (2007) Manipulation of the potassium channel Kv1.1 and its effect on neuronal excitability in rat sensory neurons. J Neurophysiol 98, 2683–2692 [PubMed: 17855588]
36. Wang FC, Bell N, Reid P, Smith LA, McIntosh P, Robertson B, and Dolly JO (1999) Identification of residues in dendrotoxin K responsible for its discrimination between neuronal K+ channels containing Kv1.1 and 1.2 alpha subunits. Eur J Biochem 263, 222–229 [PubMed: 10429207]
37. Chen Z, Hu Y, Hong J, Hu J, Yang W, Xiang F, Yang F, Xie Z, Cao Z, Li W, Lin D, and Wu Y (2015) Toxin acidic residue evolutionary function-guided design of de novo peptide drugs for the immunotherapeutic target, the Kv1.3 channel. Sci Rep 5, 9881 [PubMed: 25955787]
38. Chandy KG, Sanches K, and Norton RS (2023) Structure of the voltage-gated potassium channel K(V)1.3: Insights into the inactivated conformation and binding to therapeutic leads. Channels (Austin) 17, 2253104 [PubMed: 37695839]
39. Manville RW, Alfredo Freites J, Sidlow R, Tobias DJ, and Abbott GW (2023) Native American ataxia medicines rescue ataxia-linked mutant potassium channel activity via binding to the voltage sensing domain. Nat Commun 14, 3281 [PubMed: 37280215]
40. Salpietro V, Galassi Deforie V, Efthymiou S, O'Connor E, Marce-Grau A, Maroofian R, Striano P, Zara F, Morrow MM, Group SS, Reich A, Blevins A, Sala-Coromina J, Accogli A, Fortuna S, Alesandrini M, Au PYB, Singhal NS, Cogne B, Isidor B, Hanna MG, Macaya A, Kullmann DM, Houlden H, and Mannikko R (2023) De novo KCNA6 variants with attenuated K(V) 1.6 channel deactivation in patients with epilepsy. Epilepsia 64, 443–455 [PubMed: 36318112]
41. Wulff H, Christophersen P, Colussi P, Chandy KG, and Yarov-Yarovoy V (2019) Antibodies and venom peptides: new modalities for ion channels. Nat Rev Drug Discov 18, 339–357 [PubMed: 30728472]
42. Deer TR, Pope JE, Hanes MC, and McDowell GC (2019) Intrathecal Therapy for Chronic Pain: A Review of Morphine and Ziconotide as Firstline Options. Pain Med 20, 784–798 [PubMed: 30137539]
43. Beeton C, Pennington MW, Wulff H, Singh S, Nugent D, Crossley G, Khaytin I, Calabresi PA, Chen CY, Gutman GA, and Chandy KG (2005) Targeting effector memory T cells with a selective peptide inhibitor of Kv1.3 channels for therapy of autoimmune diseases. Mol Pharmacol 67, 1369–1381 [PubMed: 15665253]
44. Pardridge WM (2012) Drug transport across the blood-brain barrier. J Cereb Blood Flow Metab 32, 1959–1972 [PubMed: 22929442]
45. Wu LP, Ahmadvand D, Su J, Hall A, Tan X, Farhangrazi ZS, and Moghimi SM (2019) Crossing the blood-brain-barrier with nanoligand drug carriers self-assembled from a phage display peptide. Nat Commun 10, 4635 [PubMed: 31604928]

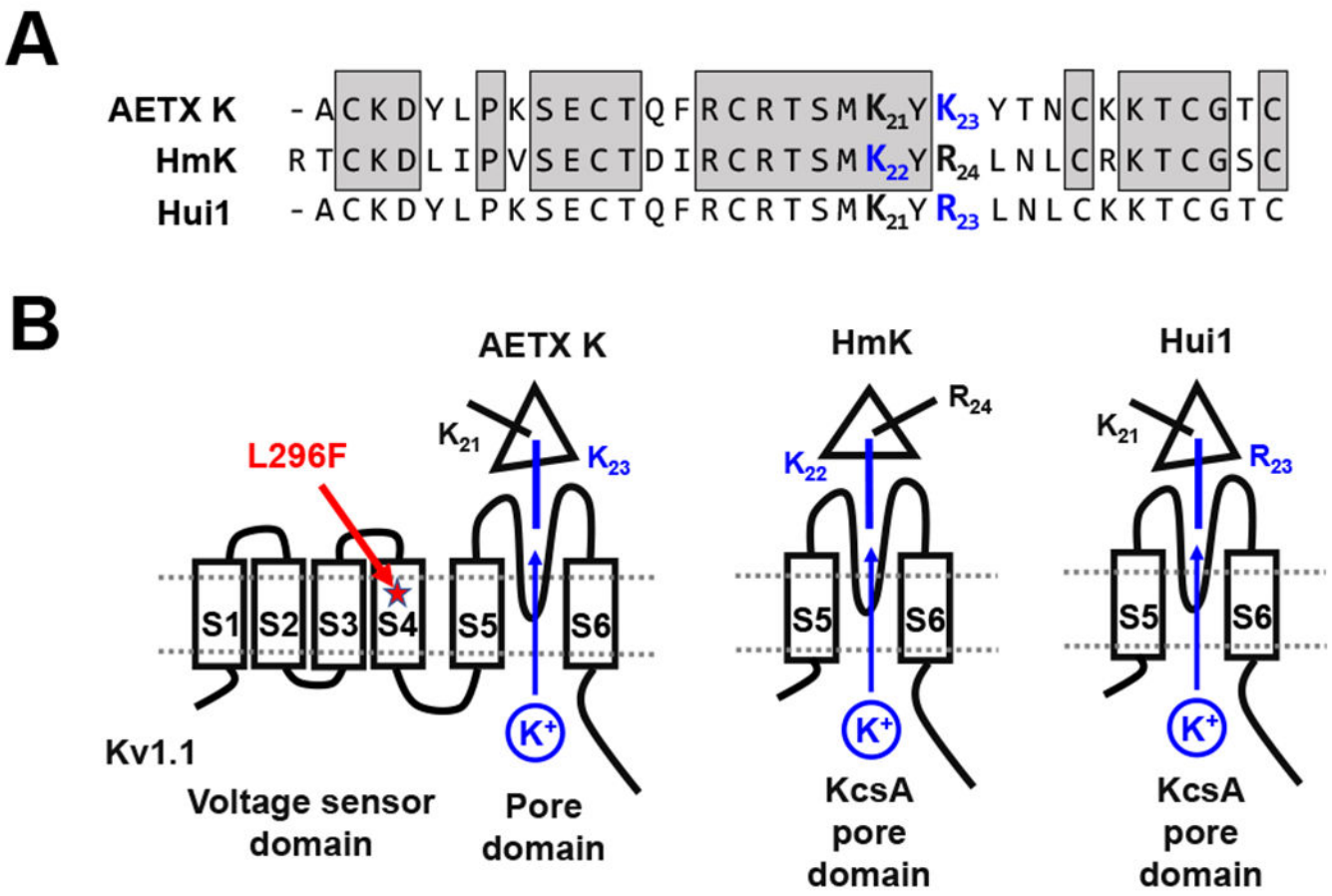

FIGURE 1. SAK1 toxins display two blocking mechanisms in the K^+ channel pore.

(A) Sequence alignment of AETX-K, HmK, and Hui1. Pore occluding residues were labeled blue. Identical residues between AETX-K and HmK were marked with grey color.

(B) Cartoon suggesting SAK1 toxin binding orientations in the Kv1.1 channel or KcsA channel external pore vestibule with Lys or Arg near the conduction pore. Left: AETX-K with Lys_{23} toward K^+ in the Kv1.1 channel pore. The epilepsy-associated gain-of-function mutation L296F (shown in red) locates at the S4 transmembrane segment in the voltage sensor domain of the Kv1.1 channel. Middle: HmK with Lys_{22} toward K^+ in the KcsA channel pore as described before (12). Right: Hui1 with Arg_{23} toward K^+ in the KcsA channel pore as described before (10).

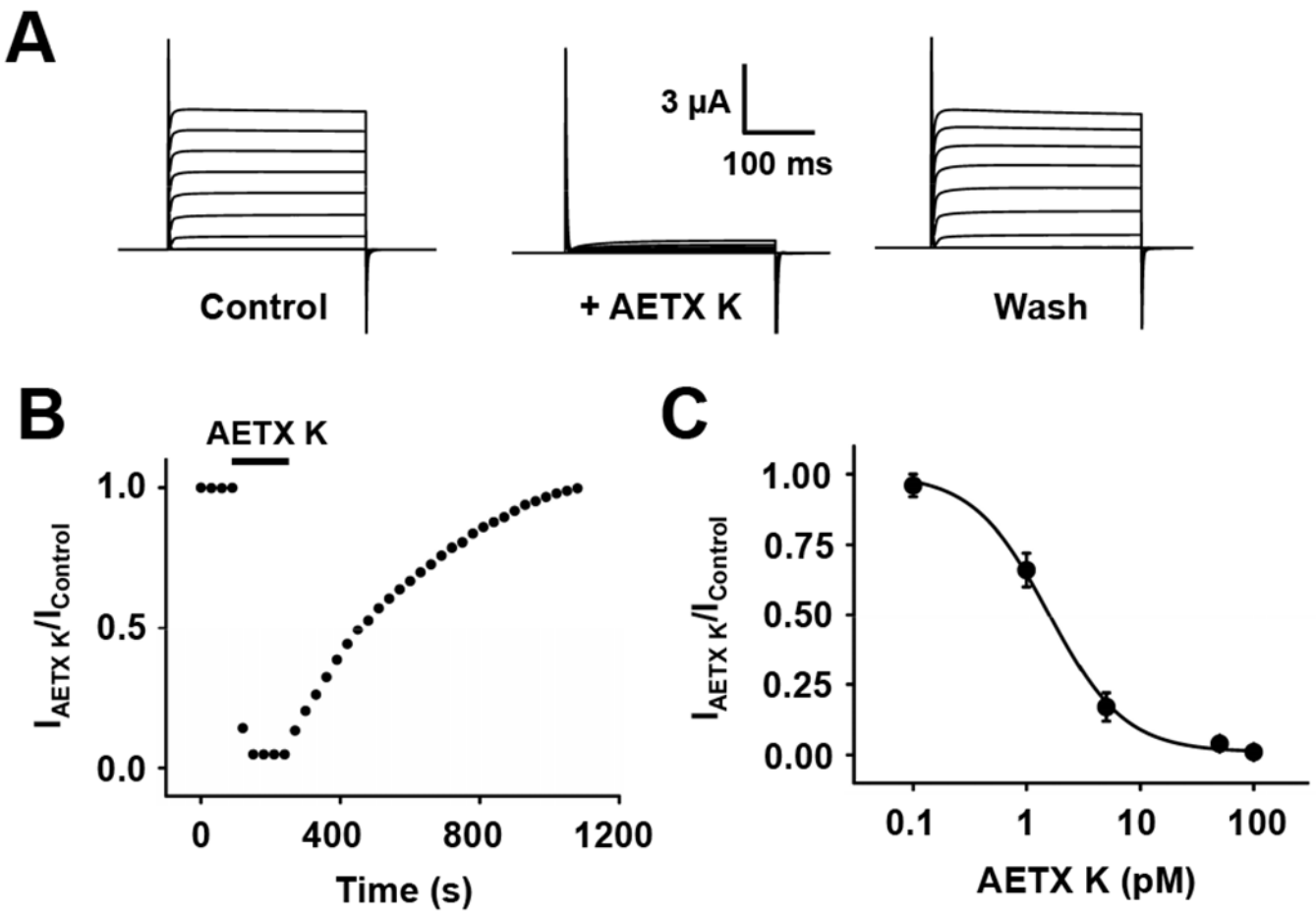

FIGURE 2. AETX-K peptide blocks Kv1.1 with low picomolar affinity.

Kv1.1 channels were expressed in oocytes and studied by two-electrode voltage clamp (TEVC) to assess equilibrium inhibition and kinetic blocking parameters using a holding voltage of −100 mV, 300-ms test pulses, and a 5-s interpulse interval, n = 5–12 cells for each condition. Values are mean ± SEM. Some error bars are smaller than symbols.

(A) Representative current traces for Kv1.1 channels at steady state before (Control), in the presence of 50 pM AETX-K, and after toxin washout (Wash) with steps of 20 mV from −100 mV to 80 mV.

(B) The time course for block and unblock of Kv1.1 on acute application (bar) and washout of 50 pM AETX-K. Peak currents recorded at 0 mV; every sixth point is shown.

(C) Dose–response relationships for AETX-K inhibition of Kv1.1 studied as in *B* and fit to the Hill equation (Materials and Methods).

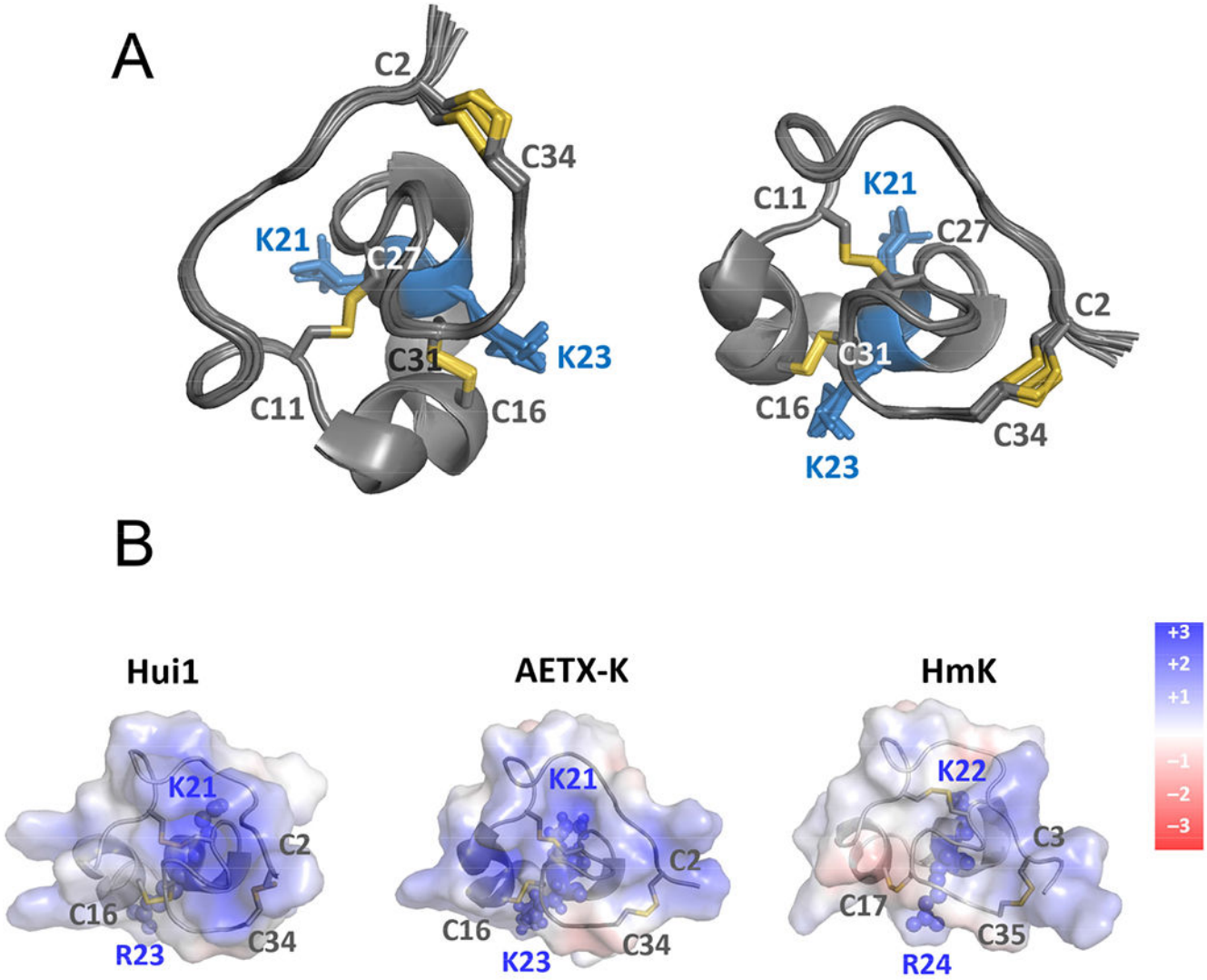

FIGURE 3. Structure of AETX-K as determined by NMR.

(A) Superposition of 23 low-energy NMR structures of AETX-K. Shown are AETX-K with the first helix head-on (left) and in channel-binding pose with Lys_{23} pointing downward (right). Disulfide bonds are highlighted in yellow and sidechains of Lys_{21} and Lys_{23} in blue. **(B)** Electrostatic surface rendering of toxins Hui1 (left), AETX-K (middle) and HmK (right) in aligned orientations according to interpolated charge (red/blue = negative/positive). Sidechains of Lys_{21} and Lys_{23} are highlighted as blue spheres.

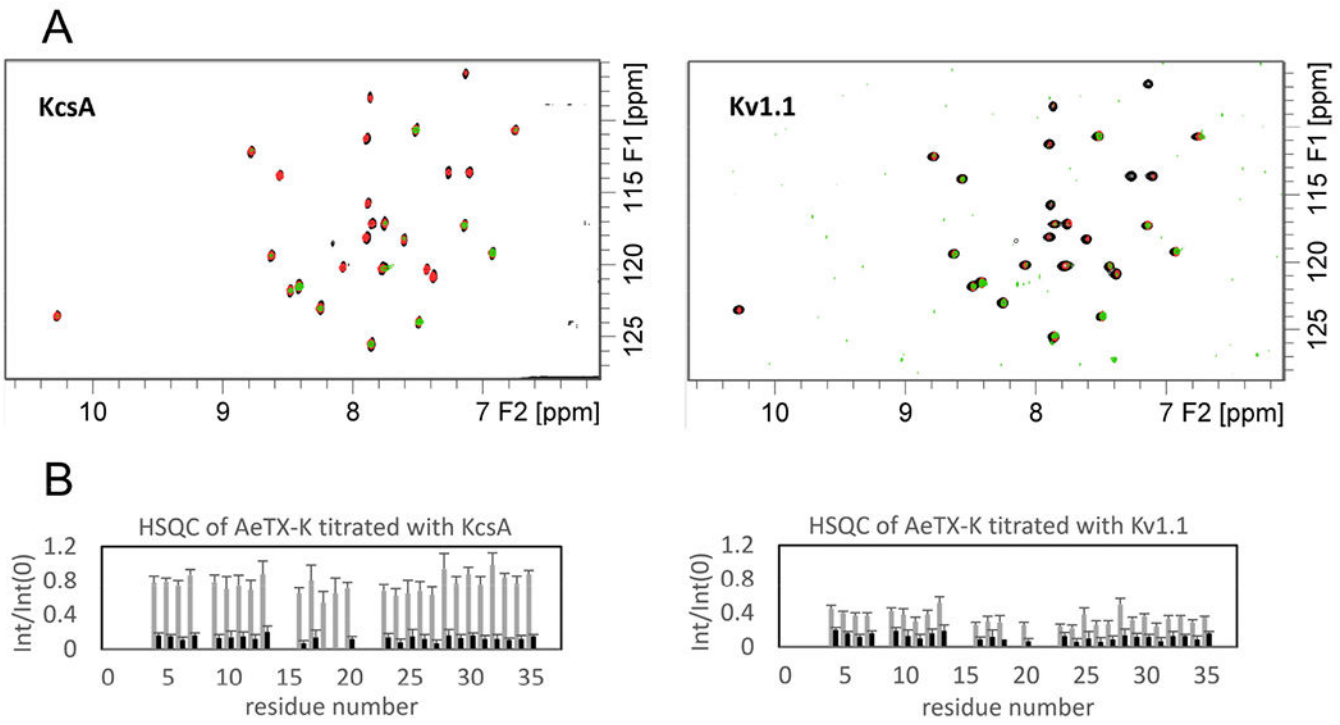

FIGURE 4. Interaction of AETX-K with KcsA and Kv1.1 are revealed by NMR.

(A) Interaction of KcsA (left) and chimeric Kv1.1 (right) with AETX-K followed by $^{15}N,^{1}H$-HSQC spectra without the LPN-embedded channel (black) and with 0.33 eq. (red) and 1.0 eq. (green) of channel. Increased weakening of peak intensity reflects stronger affinities.

(B) Summary of intensity decreases along the AETX-K sequence. Grey (dark grey) bars indicate the normalized intensity (in comparison to peaks prior to addition of channel) at 0.33 (1.00) mol:mol channel equivalents. Errors were estimated from S/N levels in all spectra.

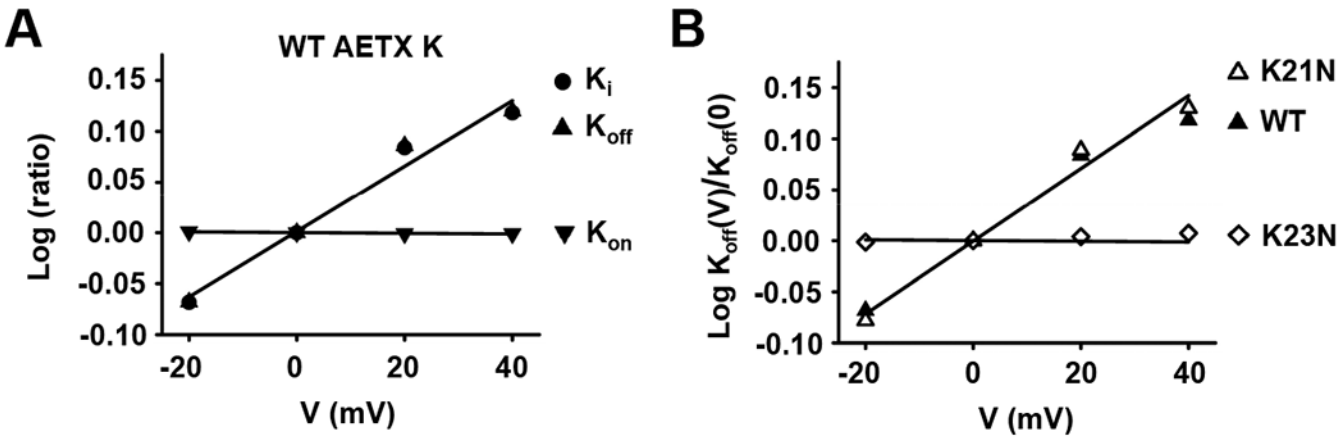

FIGURE 5. AETX-K-Lys$_{23}$ is responsible for voltage-dependent dissociation.

Kv1.1 channels were expressed in oocytes and studied by TEVC as indicated in Figure 2. n = 5–12 cells for each condition. Values are mean ± SEM. Some error bars are smaller than symbols.

(A) Effect of voltage on AETX-K blocking kinetics of Kv1.1 channels. Each parameter was measured with test steps from −20 mV to 40 mV and normalized to its value at 0 mV. Association and dissociation rate time constants were determined by single-exponential fits to the time course for block or unblock on acute application or washout of 50 pM AETX-K. The inhibition constant K_i was calculated from the fraction of unblocked current at equilibrium and the rate constants (Materials and Methods). The change in K_i with voltage is due to the altered dissociation rate.

(B) Effect of voltage on dissociation rate of Kv1.1 by AETX-K mutants. K_{off} for each toxin was determined from −20 mV to 40 mV based on the single-exponential fits to the time course for unblock on acute application or washout of 50 pM AETX-K, 5 μM AETX-K-K21N and 500 nM AETX-K-K23N and plotted as a ratio to the values at 0 mV.

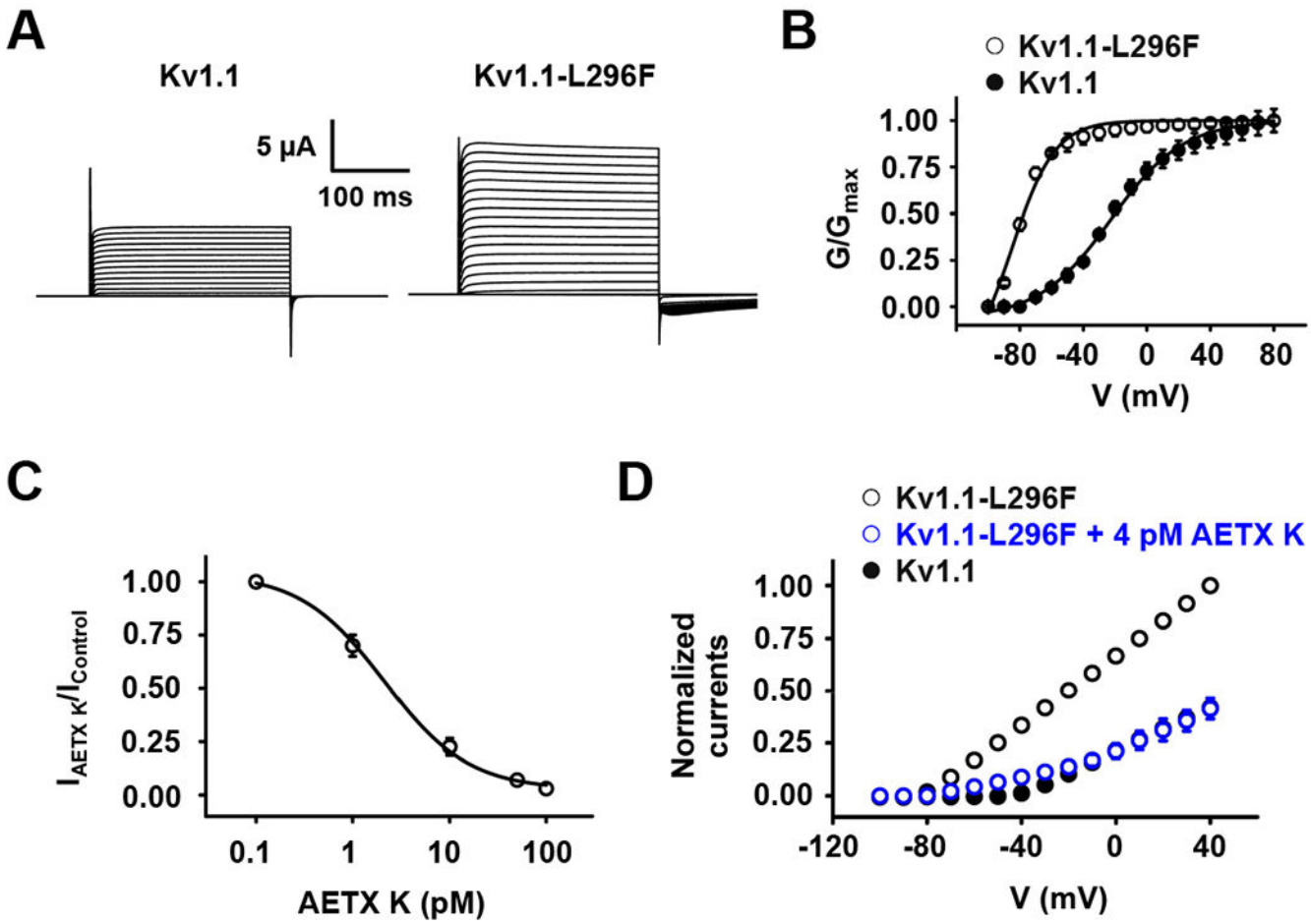

FIGURE 6. AETX-K inhibits Kv1.1-L_{296}F channels effectively.

Kv1.1 and Kv1.1-L_{296}F channels were expressed in oocytes and studied by TEVC as indicated in Figure 2. n = 5–12 cells for each condition. Values are mean ± SEM. Some error bars are smaller than symbols.

(A) Representative current traces for Kv1.1 and Kv1.1-L296F channels with steps of 10 mV from −100 mV to 80 mV.

(B) Conductance-voltage (G-V) relationship for Kv1.1 and Kv1.1-L296F. Kv1.1-L296F channels showed a −59 ± 4 mV shift in half-maximal activation voltage ($V_{1/2}$) compared to wild-type Kv1.1. Curves fit to a Boltzmann equation (Materials and Methods).

(C) Dose–response relationships for AETX-K inhibition of Kv1.1-L296F studied as in Figure 2 and fit to the Hill equation (Materials and Methods).

(D) Voltage-voltage (I-V) relationship for Kv1.1, Kv1.1-L296F, and Kv1.1-L296F with incubation of 4 pM AETX-K.

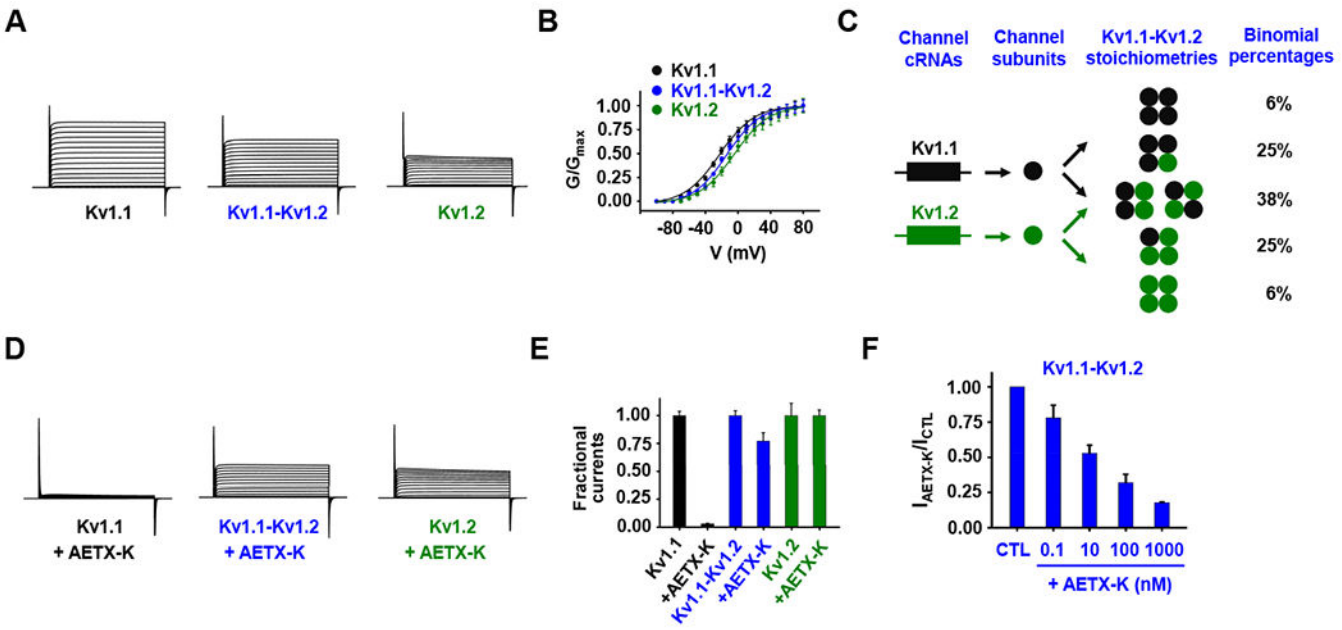

FIGURE 7. AETX-K blocks mixed populations of Kv1.1-Kv1.2 channels.

Kv1.1 and Kv1.2 channels, and Kv1.1-Kv1.2 heterotetrameric channels formed by a cRNA ratio of 50%:50% were expressed in oocytes and studied by TEVC as indicated in Figure 2. n = 3–12 cells for each condition. Values are mean ± SEM. Some error bars are smaller than symbols.

(A) Representative current traces for Kv1.1, Kv1.1-Kv1.2, and Kv1.2 channels with steps of 10 mV from −100 mV to 80 mV.

(B) G-V relationship for Kv1.1, Kv1.1-Kv1.2, and Kv1.2. Curves fit to a Boltzmann equation (Materials and Methods).

(C) After co-expression, Kv1.1 and Kv1.2 subunits assemble into tetrameric assembled channels with five different subunit stoichiometries. The theoretical percentages of expression of the five different stoichiometries of assembled channels can be calculated with the binomial equation (Materials and Methods), assuming that equal numbers of Kv1.1 and Kv1.2 subunits randomly assemble into tetrameric channels, each with equal probability to reach the membrane surface.

(D) Representative current traces for Kv1.1, Kv1.1-Kv1.2, and Kv1.2 channels at steady state in the presence of 0.1 nM AETX-K with steps of 10 mV from −100 mV to 80 mV.

(E) Kv1.1, Kv1.1-Kv1.2, and Kv1.2 currents at the end of a test pulse to 0 mV with 100 pM AETX-K.

(F) Apparent block of Kv1.1-Kv1.2 currents with 0.1, 10, 100 and 1000 nM AETX-K. The K_i for channels with different subunit stoichiometries are summarized in Table 3.

TABLE 1.

AETX-K is a specific blocker of the Kv1.1 channel.

AETX-K and HmK peptides were synthesized and their inhibition of the indicated channels at equilibrium (K_i ± SEM) were determined by two-electrode voltage clamp (TEVC) as described in Figure 2; n = 5–12 oocytes.

	K_i (nM)	
Channels	**AETX-K**	**HmK**
Kv1.1	0.0016 ± 0.0002	0.075 ± 0.008
Kv1.2	2243 ± 187	2.5 ± 0.1
Kv1.3	1230 ± 54	3.1 ± 0.2
Kv1.5	No Block	9765 ± 1390
Kv7.2	No Block	3810 ± 554
Kv7.2/7.3	No Block	6091 ± 1020

TABLE 2.

Inhibition of Kv1.1 and the gain-of-function mutation Kv1.1-L296F by AETX-K and variants.

Equilibrium inhibition constants (K_i ± SEM) were determined by TEVC as described in Figure 2. ND, not determined; n = 5–12 oocytes.

	K_i (nM)	
Toxin	**Kv1.1**	**Kv1.1-L296F**
AETX-K	0.0016 ± 0.0002	0.0021 ± 0.0001
AETX-K-K21N	1711 ± 132	ND
AETX-K-K23N	217 ± 18	ND

TABLE 3.

Inhibition of Kv1.1-Kv1.2 channels by AETX-K.

cRNAs encoding Kv1.1 and Kv1.2 were mixed with a 1:1 ratio and injected into *Xenopus* oocytes for expression of Kv1.1-Kv1.2 channels with five different subunit stoichiometries (Figure 7E). Equilibrium inhibition constants (K_i ± SEM) for Kv1.1 and K1.2 were determined by TEVC as described in Figure 2. The K_i of AETX-K for $Kv1.1_3$-Kv1.2, $Kv1.1_2$-$Kv1.2_2$, and $Kv1.1_1$-$Kv1.2_3$ were estimated based on the fractional block at equilibrium observed when applying 0.1, 10 and 1000 nM AETX-K (**Figure 7F,** n = 3–12 oocytes), the Hill equation, and the binomial distribution assuming unbiased expression and assembly of Kv1.1 and Kv1.2. Thus, 0.1 nM AETX-K blocked 22% of the current, and we can confidently surmise that Kv1.1 was fully blocked (6% of the channels) and if blockade of $Kv1.1_2$-$Kv1.2_2$ is assumed to be poor at this low level of toxin, we can attribute the fractional block (1 - F_{un}) of $Kv1.1_3$-Kv1.2 to be (22% - 6%)/(25%) = 64% offering an estimated K_i = 0.056 nM using the Hill equation $F_{un} = (1 + [Tx]/K_i)^{-1}$ for this 3:1 heteromeric channel. Next, 10 nM AETX-K blocked 47% of the current and if we assume this concentration of toxin blocks all the Kv1.1 and $Kv1.1_3$-Kv1.2 channels, removing 31% of the current, we can attribute the fractional block (1 - F_{un}) of $Kv1.1_2$-$Kv1.2_2$ to be (47% - 31%)/(38%) = 42%, leading to an estimated K_i = 14 nM using the Hill equation for the 2:2 channels. Finally, 1000 nM AETX-K blocked 82% of the current and if we assume this concentration of toxin blocks all the Kv1.1 and $Kv1.1_3$-$Kv1.2_1$ channels, essentially all of the $Kv1.1_2$-$Kv1.2_2$ channels (~98%), and a portion of Kv1.2 (~30%) removing ~70.4% of the current, we can attribute the fractional block (1 - F_{un}) of $Kv1.1_1$-$Kv1.2_3$ to be (82% - 70.4%)/(25%) = 46.4%; this leads to an estimated K_i 1155 nM using the Hill equation. Validating the reasonableness of our estimates, we predict 100 nM AETX-K should block all the Kv1.1, $Kv1.1_3$-Kv1.2 channels, and 90% of the $Kv1.1_2$-$Kv1.2_2$ channels, 8% of the $Kv1.1_1$-$Kv1.2_3$ channels and essentially no Kv1.2 channels, yielding a 67% decrease of current, and we observe 68% of block experimentally (Figure 7F).

Channels	Percentage of channels based on binomial distribution	K_i (nM)
Kv1.1	6%	0.0016 ± 0.0002
$Kv1.1_3$-Kv1.2	25%	0.056 ± 0.006
$Kv1.1_2$-$Kv1.2_2$	38%	14 ± 2
$Kv1.1_1$-$Kv1.2_3$	25%	1155 ± 30
Kv1.2	6%	2243 ± 187